On-Ground and In-Flight Estimation of Instrument Spectral Responses in the Presence of Measurement Errors

J. El Haouari[a,b], J.-M. Gaucel[c], C. Pittet[d], J.-Y. Tourneret[a,b], and H. Wendt[b]

[a]TéSA laboratory, Toulouse, France
[b]IRIT, CNRS, University of Toulouse, Toulouse, France
[c]Thales Alenia Space Cannes, France
[d]Centre National d'Etudes Spatiales, Centre Spatial de Toulouse, Toulouse, France

ABSTRACT

Space-based remote sensing facilitates the determination of greenhouse gas concentrations, enhancing the comprehension of carbon fluxes at the Earth's surface in the context of climate change. High-resolution spectrometers, such as the CNES/UKSA MicroCarb and the upcoming ESA Copernicus Carbon Dioxide Monitoring (CO2M) spectrometers, are crucial tools for this purpose. These instruments require a precise calibration, especially regarding the relative approximation errors of the Instrument Spectral Response Functions (ISRFs). To ease ISRF estimation, parametric models such as Gaussian and Super-Gaussian models have been investigated. However, these models cannot always take into account the diversity of ISRF shapes that are encountered in practical applications. For example, in MicroCarb simulations, the expected performance is not always achieved by these two conventional ISRF estimation methods, even when there is no spectral and radiometric errors. This paper investigates a novel approach based on the sparse representation of ISRFs in a dictionary. This method decomposes the spectral responses of interest as sparse linear combinations of atoms belonging to a dictionary, which are built using representative ISRFs. This new method can be applied both for on-ground ISRF denoising, and in-flight ISRF estimation through the resolution of an appropriate inverse problem. Experiments conducted using realistic simulated datasets associated with the MicroCarb instrument are used to evaluate the performance of the proposed method for on-ground and in-flight ISRF estimation, yielding promising estimation performance compared to the state of the art.

Keywords: High-resolution spectrometer, greenhouse gas concentration, instrument calibration, Instrument Spectral Response Functions (ISRFs), sparse representations

1. INTRODUCTION

Monitoring carbon dioxide (CO_2) is critical for understanding and mitigating climate change. Accurate measurements of CO_2 concentrations are thus needed to help tracking sources and sinks of carbon at the Earth surface. High-resolution spectrometers, such as the CNES/UKSA MicroCarb and the upcoming ESA Copernicus Carbon Dioxide Monitoring (CO2M) spectrometers, are crucial tools for CO_2 monitoring. They aim to ensure the continuity of carbon measurement missions such as OCO-2 and GoSAT.[1,2] However, ensuring the accuracy of these measurements requires precise on-ground and in-flight calibration. Indeed, the optical elements within these instruments can introduce spectral distortions, leading to errors in the measurements. Spectrometers, such as MicroCarb and CO2M, consist mainly of an optical part (e.g., a slit, a telescope, and a dispersive grating) and a detector. In this configuration, the telescope projects the image of the Earth onto the spectrometer slit and then onto the detector. Each pixel of the detector is associated with a spatial direction (called ACT for ACross Track) and a specific wavelength. A binning and averaging along the ACT axis are performed to improve the Signal to Noise Ratio (SNR). For each of the two parts (optical part and detector), a response function is defined, leading to a continuous optical function and another function associated with each pixel of the detector. This results in a global response function associated with each pixel along the spectral axis, known as the Instrument Spectral Response Function (ISRF), associated with a specific wavelength. The ISRFs can vary depending on the instrument, on the central wavelength, and sometimes on the scene observed by the instrument, among other factors. For some missions, such as the MicroCarb mission, ISRFs are expected to be known with a normalized approximation error less than 1%, a challenge since wavelength variations of ISRFs can exceed this threshold.

For this mission, concentrations of O_2 and CO_2 are calculated from spectra captured in four spectral bands. The first band (B1) covers 0.7583-0.7683 μm (an O_2 band) with a spectral resolution of about 0.01 nm. Bands B2 (1.596-1.618 μm) and B3 (2.023-2.051 μm), with respective spectral resolutions of about 0.02 nm and 0.03 nm, are sensitive to CO_2 concentration and have CO_2 absorption lines.[3] The last band (B4), 1.264-1.282 μm, is a second O_2 band with a spectral resolution of about 0.02 nm, closer to the CO_2 wavelength and used for validating space-based greenhouse gas observations.[4] The dataset provided by CNES includes 1024 ISRFs associated with 1024 spectral sample intervals (SSI) for each of these bands.

During on-ground calibration, measurement errors can result in erroneous ISRFs, compromising the accuracy of gas concentration retrieval. These errors are often caused by the instrument or the measurement setup (e.g., laser scans with power or wavelength stability variation). Post-processing is therefore necessary to compensate for these errors and also mitigate noise effects to achieve accurate ISRF estimation. Once calibrated on the ground, ISRFs can be re-estimated in-flight using measured spectra from specific scenes whose "theoretical" spectrum is rather well-known scenes (e.g., Sun, Moon, cold space, uniform scenes like deserts), or by pointing toward internal calibration sources such as an internal White Light lamp or by using the closed position of the instrument to acquire dark signal.[3] Estimating the ISRFs in this context can be achieved by solving an inverse problem,[5,6] that can be affected by radiometric errors and additive noise. Therefore, it is essential to consider the different degradations to ensure accurate ISRF estimation during both ground and in-flight calibration.

To ease ISRF estimation, parametric models, including the Gaussian and Super-Gaussian models, can be used.[7] However, these models cannot always account for the diversity of ISRF shapes encountered in practical applications. For example, in MicroCarb simulations, the expected performance is not always achieved by these conventional ISRF estimation methods, even when no spectral or radiometric errors are considered. Therefore, this research investigates a novel approach based on the sparse representation of ISRFs in a dictionary. This method decomposes the spectral responses of interest as sparse linear combinations of atoms from a dictionary built using representative ISRFs. Section 2 of this paper will focus on the on-ground calibration of the instrument using a sparse representation-based method to denoise ISRFs on the ground. A first estimation of the radiometric errors will be made on-ground, assuming some prior on the ISRF. Section 3 will study the joint estimation of the ISRF and radiometric errors by solving a nonlinear inverse problem. Section 4 introduces the resolution of the joint estimation problem by considering the dependence of the ISRFs on the scene observed by the instrument. All experiments are conducted using realistic simulated datasets associated with the first band (B1) of the MicroCarb instrument to evaluate the performance of the proposed method for both ground and in-flight ISRF estimation.

2. ON-GROUND CALIBRATION

Spectrometers comprise diverse components that may introduce deterministic and random errors into the measurements. During on-ground calibration campaigns, measurement errors due to the instrument or to the measurement setup (for example laser scans with power or wavelength stability variation) can result in erroneous ISRFs. In this section, the ISRFs are first denoised using either some parametric methods[7] or the proposed denoiser based on sparse representations. In addition, the radiometric responses of the instrument are estimated from flat-field observations.

2.1 ISRF Denoising Problem

During on-ground calibration, the measurement setup can highly degrade the accuracy of the estimated ISRFs. Indeed, each ISRF point is measured independently using laser and different errors can arise from the lasers such as:

- Acquisition noise which can result in an normalized ISRF approximation error between 0.05 to 0.005.

- Power stability variation which can result in a drift that occurs as the laser power increases. The ISRF measurements can thus be vertically shifted and the shift between two measurements may be linear as the laser power increases or completely random. In practice, each ISRF point is measured independently, and as the laser power increases, a drift occurs (the ISRF points are vertically offset). The shift may be

linear or completely random between two measurements, and the degree of randomness may vary between different points.

- Wavelength stability variation which results in an error about the knowledge of the laser wavelength that may introduce horizontally shifted (i.e., irregularly sampled) measurements.
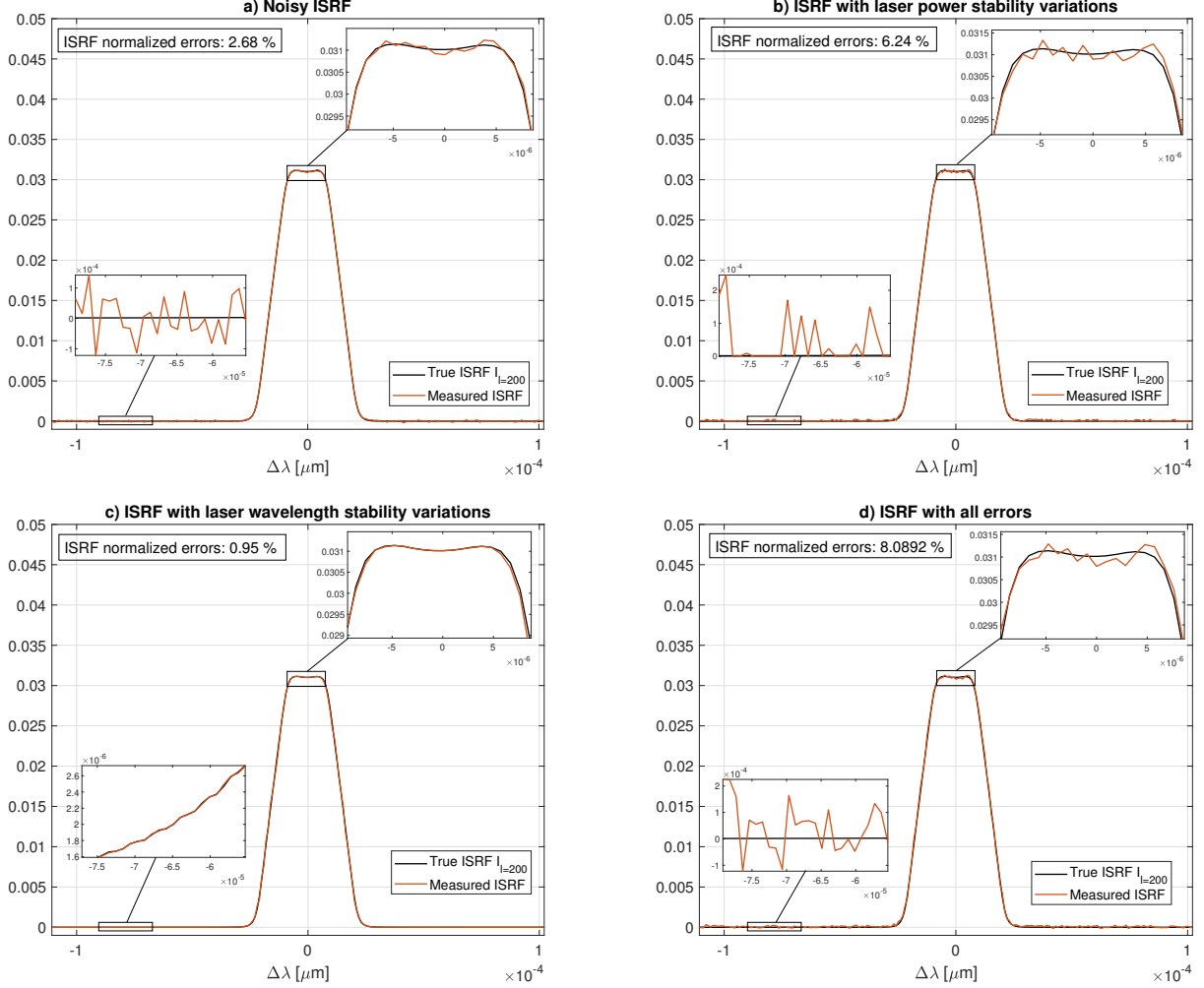

Figure 1. Examples of possible impacts of the laser on the shape of the ISRFs.

Figure 1 illustrates the different kind of errors that result from the use of these lasers. The obtained measured ISRF $\tilde{I}_l$ at the wavelength λ_l associated with the pixel l can be expressed from the true ISRF I_l as:

$$\tilde{I}_l(\lambda_l) = I_l(\lambda_l + \delta_l) + \epsilon_l, \tag{1}$$

where ϵ_l takes into account the acquisition noise and the vertical shift and δ_l is the horizontal shift for one measurement. The ISRF denoising problem can be solved by minimizing the norm of the residual the between the measurement and a model of the true ISRF. In the literature, parametric models including the Gaussian and Super-Gaussian models[7] have been extensively used to approximate ISRFs. However, these models can struggle to reach the accurate approximation of the ISRFs. Models based on sparse approximations or dictionary learning have been successfully used for several image processing applications including denoising.[8] The use of sparse representation techniques has also been recently reported for approximating the ISRFs from measured spectra.[5] In this paper, we propose to use these representations to denoise the ISRFs. The lth measured ISRF is represented

as a vector $\tilde{\boldsymbol{I}}_l \triangleq \left[\tilde{I}_l(-\frac{N}{2}\Delta), ..., \tilde{I}_l(\frac{N}{2}\Delta) \right]^T \in \mathbb{R}^{N+1}$ in the wavelength grid Δ and is decomposed in a dictionary of atoms $\boldsymbol{\Phi} \in \mathbb{R}^{(N+1) \times N_D}$ as[5]

$$\tilde{\boldsymbol{I}}_l = \boldsymbol{\Phi}\boldsymbol{\alpha_l}, \tag{2}$$

where $\boldsymbol{\alpha_l} \in \mathbb{R}^{N_D}$ is a sparse vector that can be obtained by solving the following optimization problem

$$\arg\min_{\boldsymbol{\alpha_l}} ||\tilde{\boldsymbol{I}}_l - \boldsymbol{\Phi}\boldsymbol{\alpha_l}|| + \mu||\boldsymbol{\alpha}_l||_0. \tag{3}$$

The algorithm used to solve this problem is the Orthogonal Matching Pursuit (OMP).[9, 10] The estimates obtained using OMP are compared with the estimates resulting from Gaussian and Super-Gaussian parameterizations, as suggested in.[7] The results are presented in Fig. 2 and lead to the following observations. The Super-Gaussian method achieves a lower ISRF approximation error than the Gaussian method. However, the best results are obtained using the sparse representation-based method , with a normalized ISRF approximation error below 1%, indicating the efficacy of the method for denoising the ISRFs.
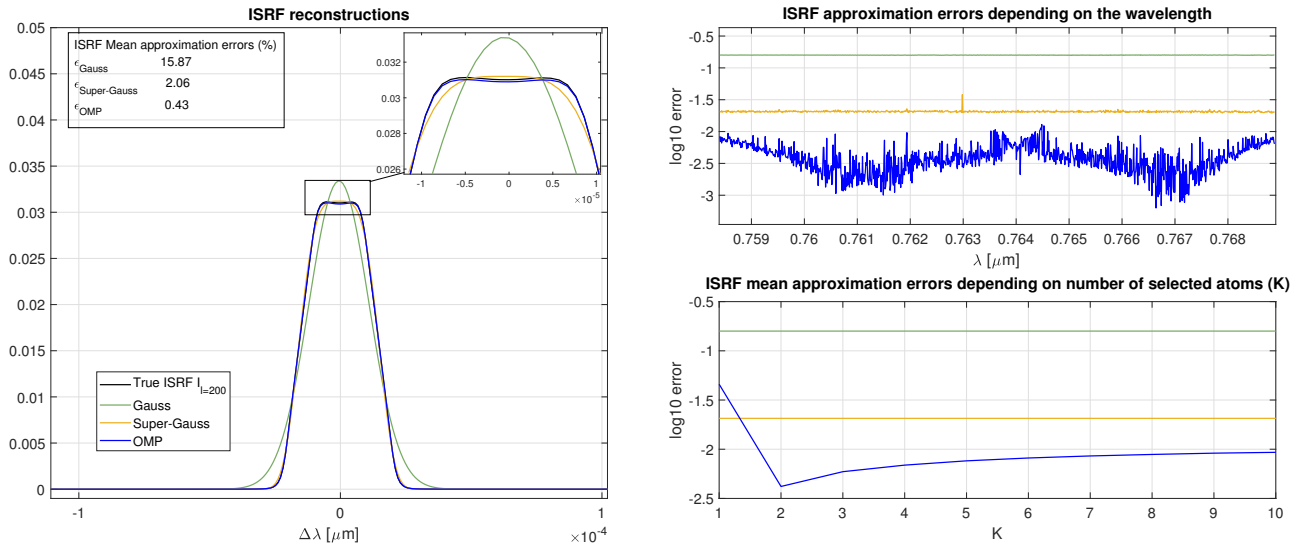

Figure 2. Solving the ISRF denoising problem using either Gaussian, Super-Gaussian or the OMP algorithm.

2.2 Pre-Flight Radiometric Calibration of the Instrument

As illustrated in Fig. 3, the radiometric errors can widely distort the true spectrum and need to be estimated. These errors depend on the pixel of the detector and thus on the associated wavelength. There is one function describing the distortion to estimate per wavelength. In the literature, the radiometric errors are frequently assumed to be polynomials.[11, 12] Indeed, the preflight calibration of OCO-2 was conducted in a thermal vacuum chamber (TVAC chamber) with the use of multiple external scenes to obtain a range of radiance levels. Fits were performed using polynomial orders of one to five to estimate the radiometric errors.[11] Choosing a third order polynomial proved to be effective in terms of residual fits also on the MicroCarb data. From a more theoretical perspective, another indication of the usefulness of polynomial functions can be derived. Indeed, it is well-established that any continuous function defined on an interval can be uniformly approximated by a polynomial function (in accordance with the Stone-Weierstrass approximation theorem[13]). During the on-ground calibration phase, precise values of the ISRFs are not required. The measured spectrum is denoised by taking several acquisitions of the same luminance. Subsequently, flat-field observations are used to estimate the radiometric response associated with each wavelength. The results in terms of polynomial approximations of order 3 are displayed in Fig. 4 for three different pixels, showing a good match between the measurements

and the polynomial fit. A correction process, that will be more detailed in Sec. 3, is then used to retrieve the corrected spectrum, displayed in blue in Fig. 3, assessing the good performance of the method in correcting the measured spectrum.
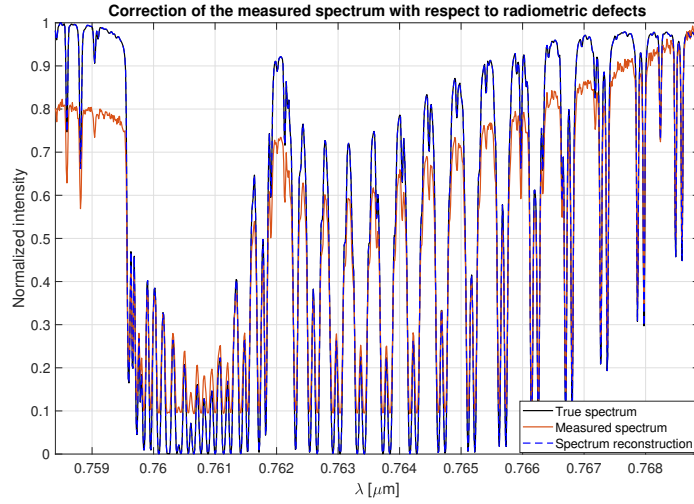

Figure 3. On-ground reconstruction of the true spectrum from the measured spectrum in presence of radiometric errors.
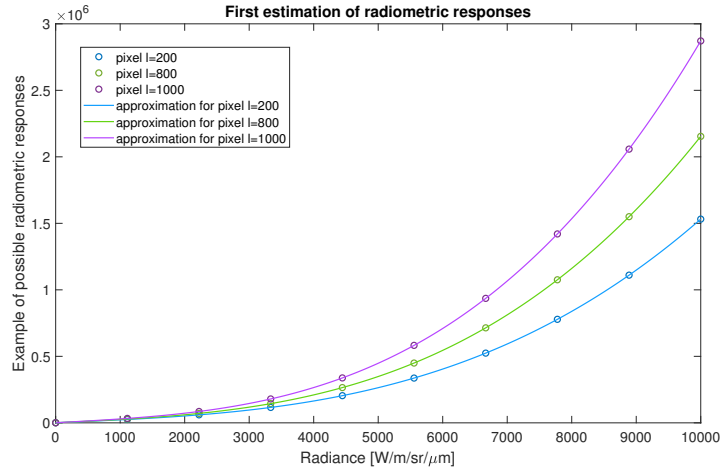

Figure 4. On-ground estimation of the radiometric responses - Assuming polynomial shape.

3. IN-FLIGHT CALIBRATION

For the in-flight calibration of the MicroCarb instrument, the payload is composed of a Pointing and Calibration Subsystem (PCS).[3] This system includes a scan mirror, which allows the instrument to point towards the Earth for the scientific acquisitions, or towards internal or external calibration sources (lamp, Moon, Sun).

The principle of ISRF estimation during in-flight estimation is to determine the ISRFs $I_l \in \mathbb{R}^{N+1}$ for each wavelength λ_l that minimize some similarity measure between the measured spectrum and a "theoretical" spectrum convolved with the ISRF. This theoretical spectrum is the spectrum obtained at the entrance of the instrument and is assumed to be well-known during the calibration process. To estimate these ISRFs, which can vary along the wavelength bands, an observation window $\mathcal{W}_l = \left\{ \lambda_{l-\frac{L}{2}}, ..., \lambda_{l+\frac{L}{2}} \right\}$ of $L + 1$ observations can be used.[5] This amounts to solving a linear inverse problem that can be solved using a sparse representation of the

ISRF in a dictionary:

$$\boldsymbol{s}_l = \boldsymbol{S}_{th,l}\boldsymbol{I}_l = \boldsymbol{S}_{th,l}\boldsymbol{\Phi}\boldsymbol{\alpha}_l, \tag{4}$$

where $\boldsymbol{s}_l \in \mathbb{R}^{L+1}$ is the measured spectrum in the observation window without radiometric or spectral errors, and $\boldsymbol{S}_{th,l} \in \mathbb{R}^{(L+1)\times(N+1)}$ is a matrix containing the theoretical spectra interpolated at the window wavelengths. However, the spectrum $\boldsymbol{s}_l$ is not the actual measured spectrum since radiometric errors are not considered in (4) and can highly affect the measurement, as highlighted in Fig. 3. These radiometric errors thus need to be taken into account during this calibration.

3.1 Experimental Setup and Formulation of the nonlinear inverse problem

Similarly to the on-ground calibration, the radiometric errors are modeled as polynomials that are wavelength dependent and are applied to the spectrum $\boldsymbol{s}_l$. The resulting problem is ill-posed, as a single measurement is insufficient for estimating the coefficients of the $L + 1$ polynomials in $\mathcal{W}_l$. Consequently, multiple theoretical spectra are required for estimation purposes. The relationship between the spectrum $s_{l',q}$ and the measured spectrum $x_{l',q}$ for $l' \in \mathcal{W}_l$ and for the $q \in \{1, ..., Q\}$-th theoretical spectrum can be expressed:

$$x_{l',q} = f_{l'}(s_{l',q}) + \epsilon_{l'} = \sum_{p=0}^{P} d_{l',p}(s_{l',q})^p + \epsilon_{l'} \quad \forall\, l' \in \mathcal{W}_l \quad \forall\, q = 1, ..., Q, \tag{5}$$

where P is the polynomial order and $\epsilon_{l'}$ is a Gaussian additive noise.

Our novel approach has recently been introduced in [6] and has demonstrated potential for the joint estimation of ISRFs and radiometric errors. The method employs an iterative approach that alternates between the estimation of radiometric responses, assuming polynomial models, the correction of these errors, and the estimation of ISRFs based on a sparse representation in a dictionary. In a first step, ISRFs are estimated from measured spectra under the assumption that there are no radiometric errors. Subsequently, radiometric errors are estimated for each wavelength of the window $\mathcal{W}_l$ at each iteration from the previous ISRF estimates by solving $L + 1$ least-squares problems. Then, the measured spectra are corrected using the estimated coefficients $d_{l',p} \;\forall\, l' \in \mathcal{W}_l \;\forall\, p \in \{0, ..., P\}$, thereby enabling a new estimate of the ISRF from the corrected spectra. Further theoretical information on our estimation method can be found in [6].

In the simulations, the estimation of both the ISRFs and the radiometric responses is conducted using a limited number of known theoretical spectra from the calibration sources (internal/dark flat-field, sum or other well known and stable atmospheric scenes). The SNR was set to 55 dB. The dictionary used for the sparse representation of the ISRFs was constructed using $N_{\mathrm{D}} = 25$ singular vectors, associated with the largest singular values of a singular value decomposition (SVD) of 103 out of 1024 (10%) ISRF examples, which were simulated for the selected band. The size of the observation window was set to $L = 80$, and the polynomial order is $P = 3$. In contrast to the 100 iterations used in previous research,[6] the present simulations presented in this paper were obtained with 200 iterations. This adjustment is motivated by the fact that a reduced number of theoretical spectra are available for in-flight calibration in the present context.

3.2 Joint Estimation of ISRFs and Radiometric Errors

The results are presented in terms of the reconstruction of the measured spectrum without radiometric errors, the estimation of the ISRFs, and the estimation of the radiometric responses. Two different scenarios are considered. In the first scenario, referred to as linear case, the radiometric errors are not generated. The second scenario generates the radiometric errors for each wavelength and is referred to as the nonlinear case. The performance of the sparse representation-based method is evaluated in Sec. 3.2.1 and 3.2.2 through the examination of both the linear case, which represents an optimal scenario, and the nonlinear case, which reflects a realistic scenario involving radiometric errors. Section 3.2.3 presents the results related to the polynomial approximations of the radiometric errors.

3.2.1 Spectral reconstruction from the degraded measured spectrum using the iterative algorithm

The performance is first evaluated at the end of the iterative algorithm in terms of residual error between the normalized measured spectrum without radiometric errors and its normalized reconstruction in the two different scenarios. Figure 5 compares the reconstructions of the true measurements and the corresponding residuals for the two scenarios.
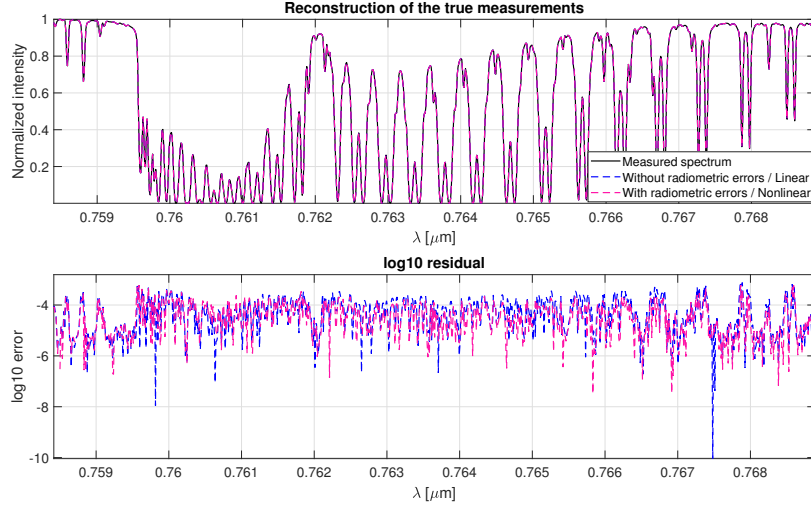

Figure 5. In-flight reconstruction of the measured spectrum without radiometric errors or in presence of radiometric errors, assuming a polynomial shape.

A first observation is that in the two scenarios, the proposed method enables the accurate retrieval of the spectrum without radiometric errors. Furthermore, in presence of radiometric errors, the measured spectrum is effectively well corrected, and the residual errors remain at a low level. Finally, an outstanding result is that the residual errors obtained in the two cases are similar, which confirms the good performance of the iterative method.

3.2.2 ISRF Estimation using a Sparse Representation

The performance is then evaluated in terms of normalized absolute error for the ISRF approximation (at a given wavelength), i.e.,

$$E_l = \sum_{n=1}^{N+1} |\boldsymbol{I}_l[n] - \hat{\boldsymbol{I}}_l[n]| / \sum_{n=1}^{N+1} \boldsymbol{I}_l[n]. \tag{6}$$

Figure 6 shows an example of estimated ISRF (associated with pixel $l = 200$ of the detector) in the absence and presence of radiometric errors. The approximation errors for both cases are displayed for a fixed number of selected atoms ($K = 4$) or averaged for all ISRFs in the band while the value of K varies.

Both methods yield satisfactory results, with the lowest average approximation errors obtained using $K = 4$ atoms in the dictionary. For this value of K, the ISRF approximation errors for all wavelengths λ_l are below 1% and occasionally reach 0.1%. In the presence of radiometric errors, the ISRF approximation error is observed to be larger at the spectral lines (around $0.763\mu m$) than at the continuum of the spectrum (around $0.759 \mu m$). This observation is likely due to the fact that radiometric errors are more challenging to estimate in the spectral lines than in the continuum. Conversely, in the absence of radiometric errors, it is more feasible to estimate the ISRFs at the spectral lines than in the continuum.
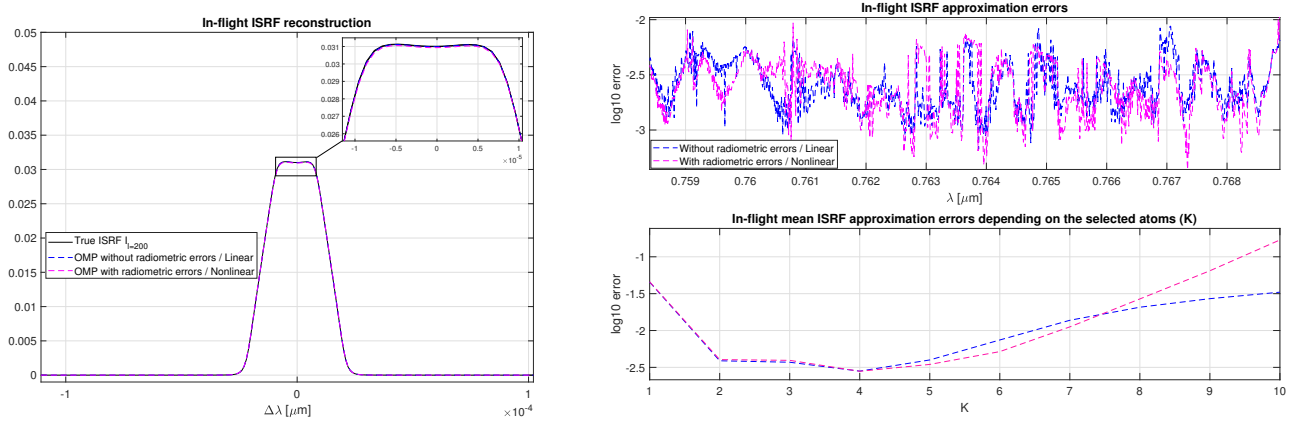
Figure 6. In-flight estimation of the ISRFs using the OMP algorithm without radiometric errors or in presence of radiometric errors, assuming a polynomial model.

3.2.3 Radiometric Error Estimation using Polynomial Fitting

Figure 7 shows three illustrative examples of polynomial curves used for modeling radiometric errors for three distinct pixels, alongside the corresponding estimates obtained using the iterative algorithm. The figure shows demonstrates the efficiency of the iterative approach in estimating the radiometric responses of the instrument.
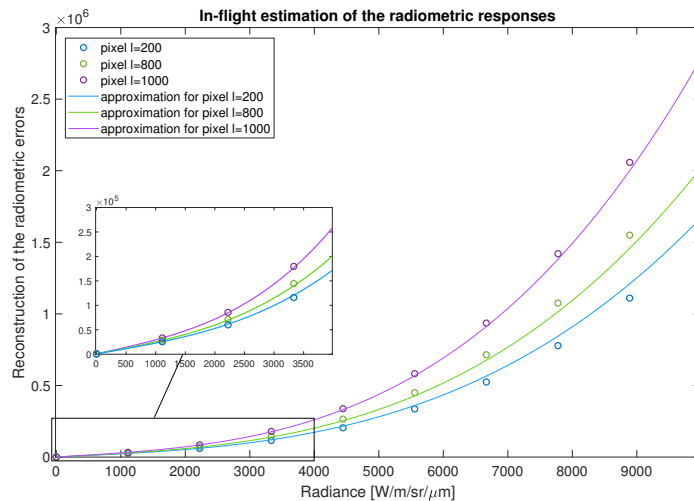

Figure 7. In-flight estimation of the radiometric errors for three different pixels, assuming a polynomial of order $P = 3$.

4. DEPENDENCE OF THE ISRF ON THE SCENE

One particularity of the MicroCarb mission is the dependence of the ISRF on the scene observed by the instrument.[5] Indeed, for some scenes, the illumination of the instrument slit is not uniform, which can result in alterations to the shape of the associated ISRF, leading to a more asymmetric outcome. Furthermore, radiometric errors are also present in this context and have the potential to significantly alter the measured spectrum, thereby influencing the ISRF estimation. We thus propose an evaluation of the iterative algorithm on ISRFs associated with eight different scenes. Moreover, as indicated in previous work,[5] a novel dictionary must be employed in some cases, comprising the initial 103 examples of ISRFs from uniform scenes and three additional

ISRFs from non-uniform scenes (out of 24). This approach has demonstrated superior performance in the linear case compared to a dictionary comprising only uniform scenes.[5] The size of the dictionary remains fixed at $N_D = 25$. The results are presented in Fig. 8 and demonstrate the efficiency of the iterative method, even in this challenging scenario. Indeed, the method achieves errors below 1% for all eight scenes and three FOVs, sometimes approaching 0.1%. The lowest ISRF approximation error is obtained using $K \in \{3, 4, 5, 6\}$ atoms, depending on the scene observed and the FOV. Figure 8 illustrates the estimation of an ISRF in presence of radiometric errors as compared to the ground truth for the horizontal coast profile. This particular scene presents the greatest variability in ISRF shape, representing a challenging, worst-case scenario. The results demonstrate that the ISRF estimation method performs well even when accounting for radiometric errors with this particular scene.
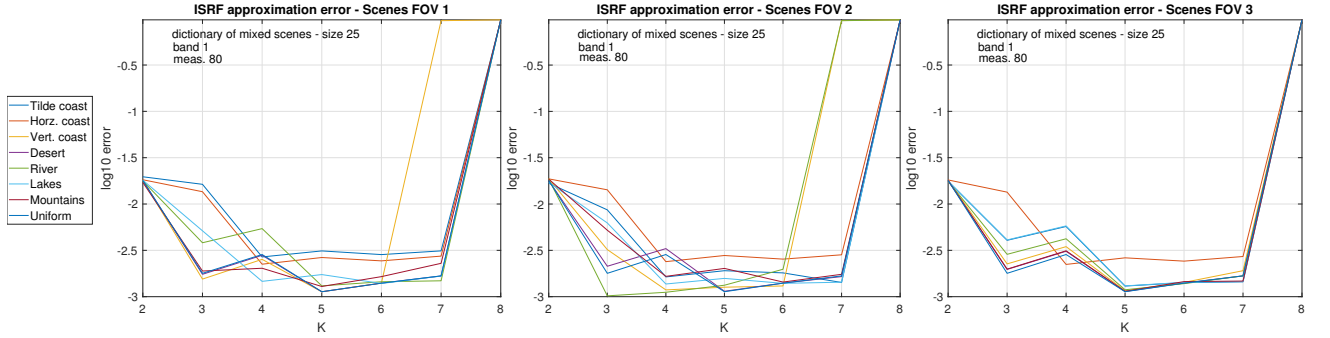

Figure 8. In-flight ISRF estimation errors for ISRFs of different scenes using the OMP algorithm in presence of polynomial radiometric errors.
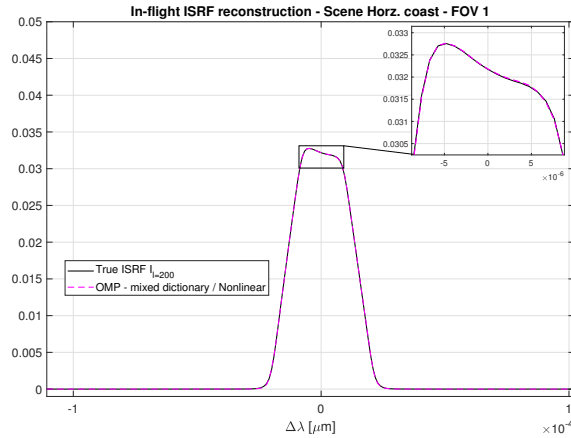

Figure 9. Example of ISRF estimation for an horizontal coast profile scene using the OMP algorithm during in-flight calibration in presence of polynomial radiometric errors.

5. CONCLUSION

This paper studies the performance of a new method for approximating the spectral response functions (ISRFs) and the radiometric responses of ground and airborne spectrometers. The ISRFs are first denoised with high accuracy for the on-ground calibration using sparse representations in a dicitonary, resulting in ISRF approximation errors less than 1%. Subsequently, the radiometric responses are calculated assuming a polynomial model. During in-flight calibration, both the ISRFs and the radiometric errors are re-estimated using multiple well-known theoretical spectra (Sun, Moon, uniform scenes, flat-field observations, dark signal, etc.) by solving nonlinear inverse problems. The joint estimation of radiometric errors and ISRFs is performed using an iterative

process investigated in [6]. This process alternates between least-squares estimation of radiometric errors, correction of radiometric errors by searching the roots of appropriate polynomials, and estimation of sparse vectors using the OMP algorithm. The simulations conducted in this work indicate that the proposed ISRF estimation method works well in the scenario where there is no radiometric errors and when these errors are generated, the proposed iterative method is nearly as effective as the method developed for measurements not affected by radiometric errors. Another promising result is the adaptability of the joint estimation method, which considers the ISRF dependence on the scene. This allows for accurate estimation in eight different scenes.

Future work will include further consideration of the impact of spectral sampling on the ISRF denoising process and on the potential use of these denoised ISRFs as a reference in the construction of the dictionary. Moreover, additional factors that may contribute to degradation during in-flight calibration have been identified, including the aging of the lamp, the accuracy of theoretical spectra, and straylight. These factors have been identified as potential sources of error. Additionally, an imperfect knowledge of the wavelength at which the ISRFs are centered can result in spectral shifts of the spectral measurements, which will consequently impact the estimation of the ISRFs in the inverse problem. A detailed analysis of these factors will be conducted to assess their impact on the overall accuracy of the method. Another avenue for exploration is the potential interest of machine learning methods, such as neural networks, for learning all the different forms of degradation and estimating the ISRF.

REFERENCES

[1] Eldering et al., A., "The orbiting carbon observatory-2 early science investigations of regional carbon dioxide fluxes," *Science* **358**, eaam5745 (Oct. 2017).

[2] Imasu et al., R., "Greenhouse gases Observing SATellite 2 (GOSAT-2): mission overview," *Prog. Earth Planet. Sci.* **10**, 33 (July 2023).

[3] Cansot, E., Pistre, L., Castelnau, M., Landiech, P., Georges, L., Gaeremynck, Y., and Bernard, P., "Micro-Carb instrument, overview and first results," *Proc. SPIE 12777, Inf. Conf. Space Optics* **12777**(1277734), 1–13 (2022).

[4] Bertaux, J.-L., Hauchecorne, A., Lefèvre, F., Bréon, F.-M., Blanot, L., Jouglet, D., Lafrique, P., and Akaev, P., "The use of the $1.27 \mu m$ o_2 absorption band for greenhouse gas monitoring from space and application to microcarb," *Atmos. Meas. Tech.* **13**(6), 3329–3374 (2020).

[5] El Haouari, J., Gaucel, J.-M., Pittet, C., Tourneret, J.-Y., and Wendt, H., "Estimation of instrument spectral response functions using sparse representations in a dictionary," in [*IEEE Int. Geosci. Remote Sens. Symp. (IGARSS 2024) , to be published*], (July 2024).

[6] El Haouari, J., Tourneret, J.-Y., Wendt, H., Gaucel, J.-M., and Pittet, C., "Estimation of instrument spectral response functions in presence of radiometric errors," in [*IEEE European Signal Process. Conf. (EUSIPCO 2024) , to be published*], (2024).

[7] Beirle, S., Lampel, J., Lerot, C., Sihler, H., and Wagner, T., "Parameterizing the instrumental spectral response function and its changes by a super-Gaussian and its derivatives," *Atmos. Meas. Tech.* **10**(2), 581–598 (2017).

[8] Donoho, D. L., Elad, M., and Temlyakov, V. N., "Stable recovery of sparse overcomplete representations in the presence of noise," *IEEE Trans. Inf. Theory* **52**(1), 6–18 (2005).

[9] Mallat, S. G. and Zhang, Z., "Matching pursuits with time-frequency dictionaries," *IEEE Trans. Signal Process.* **41**(12), 3397–3415 (1993).

[10] Pati, Y. C., Rezaiifar, R., and Krishnaprasad, P. S., "Orthogonal matching pursuit: recursive function approximation with applications to wavelet decomposition," in [*Proc. Asilomar Conf. Signals Syst. Computers*], 40–44 (Nov. 1993).

[11] Rosenberg, R., Maxwell, S., Johnson, B. C., Chapsky, L., Lee, R. A. M., and Pollock, R., "Preflight Radiometric Calibration of Orbiting Carbon Observatory 2," *IEEE Trans. on Geosci. Remote Sens.* **55**(4), 1994–2006 (2017).

[12] Keller, G. R., Rosenberg, R. A., Spiers, G. D., Yu, S., Merrelli, A., O'Dell, C. W., Lee, R. A., Crisp, D., Eldering, A., and Chatterjee, A., "Inflight Radiometric Calibration and Performance of the Orbiting Carbon Observatory 3 for Version 10 Products," *IEEE Trans. on Geosci. Remote Sens.* **60**, 1–18 (2022).

[13] Stone, M. H., "The generalized Weierstrass approximation theorem," *Mathematics Magazine* **21**, 167 (1948).